OATAO

Open Archive Toulouse Archive Ouverte

Open Archive Toulouse Archive Ouverte (OATAO)

OATAO is an open access repository that collects the work of Toulouse researchers and makes it freely available over the web where possible

This is an author's version published in: **http://oatao.univ-toulouse.fr/23697**

Official URL:

https://microscopy-analysis.com/magazine/issues/cryo-tem-and-image-analysis-polymer-nanoparticle-dispersions

---

To cite this version:

Durrieu, Vanessa and Putaux, Jean-Luc and Passas, Raphaël and Gandini, Alessandro *Cryo-TEM and Image Analysis of Polymer Nanoparticle Dispersions.* (2004) Cryoelectron Microscopy, 18 (1). 19-21. ISSN 0958-1952

Any correspondence concerning this service should be sent to the repository administrator: tech-oatao@listes-diff.inp-toulouse.fr

Cryo-TEM and Image Analysis of Polymer Nanoparticle Dispersions

Vanessa Durrieu[1], Jean-Luc Putaux [2], Raphaël Passas[1] and Alessandro Gandini [1]
1. E.F.P.G., Grenoble, France   2. Centre de Recherches sur les Macromolécules Végétales, CNRS, Grenoble, France

ABSTRACT
Light scattering is routinely used to measure the average particle size in aqueous polymer dispersions. However, difficulties arise for polymodal populations, nanometric particles, absorbent materials or mixtures of materials with different densities. A complementary approach consists in combining cryo-TEM and image analysis. Using these techniques, we studied various polyurethane aqueous dispersions. The nanoparticles were characterised in terms of morphology and size. Average diameters, calculated using a semi-automatic image analysis procedure, were compared to those obtained from dynamic light scattering.

KEYWORDS
polymer nanoparticles, cryo-TEM, image analysis, size distribution

AUTHOR DETAILS
Dr Vanessa Durrieu, Ecole Française de Papeterie et des Industries Graphiques, Domaine Universitaire, BP 65, F-38402 St Martin d'Hères Cedex, France.
Tel : +33 476 82 69 58
Fax : +33 476 82 69 33
Email: raphael.passas@efpg.inpg.fr
        putaux@cermav.cnrs.fr

INTRODUCTION

The interest in aqueous-based resins for various applications such as coating or in the pharmaceutical field has recently increased due to the need for constant cost reductions and the necessity to control emissions of volatile organic compounds. As most polymers used in these applications are water insoluble, aqueous-based resins generally contain particles in suspension. The average particle size and size distribution are essential data on which the stability and properties of the dispersions depend [1]. Light scattering and cryo-transmission electron microscopy (cryo-TEM) have proved to be complementary techniques to characterise various natural [2] or synthetic [3] polymer nanoparticles dispersed in water. Light scattering is non-destructive and provides fast measurements in a wide range of particle size. However, it cannot analyse double populations, large distributions, absorbent materials, or mixtures of substances with different densities [4]. In this study, cryo-TEM and image analysis were combined to characterise a variety of aqueous polyurethane dispersions. The results were compared with those obtained from dynamic light scattering (DLS) experiments.

MATERIALS AND METHODS

Aqueous polymer dispersions
Polyurethane-urea dispersions were prepared according to the method described by Lahtinen et al. [5]. A polyurethane pre-polymer with reactive isocyanate chain ends was synthesised and dispersed in water. Chain extension was carried out and nanoparticles formed. Several dispersions were studied, varying the nature and proportion of the raw materials (di-isocyanates, polyols and emulsifying agents).

Light scattering
DLS was carried out using a Malvern Autosizer 2c photon correlation spectrometer (Malvern Instruments, Orsay, France) equipped with a HeNe laser (10 mW, 632.8 nm) and operated at an angle of 90°. The Z-average mean diameter $D_{Z(DLS)}$ was calculated using the cumulant analysis (standard method ISO 13321). Dispersions exhibiting a polydispersity index (as defined by the spectrometer) higher than 0.25 were discarded from our comparative study.

Cryoelectron microscopy
According to the method described elsewhere [6,7], thin liquid films of 1 mg/ml nanoparticle dispersions were prepared onto 'lacey' carbon films (Pelco, USA) and quench-frozen into liquefied ethane (Fig 1). Once transferred into a Gatan 626 cryoholder, the specimens were observed at -180°C using a Philips CM200 cryomicroscope operated at 80 kV. Micrographs were recorded on Kodak SO163 films at magnifications of 11,500 and 20,000, with a defocus of 1-2 µm.

Image analysis and size distribution
The negatives were digitised using a Kodak Megaplus CCD camera. The magnification was chosen in order to include a large number of particles in the field of view, while maintaining a sufficient resolution. A sampling rate of 2 nm/pixel was considered to be a good compromise. Contrast enhancement and semi-automatic particle measurements were performed using routines from the Optimas 6.51 software (Media Cybernetics, Inc.) [8]. The number-average diameter $\overline{D}_N$, the weight-average diameter $\overline{D}_W$, as well as a polydispersity index P_D were defined using the following formulas:

$$\overline{D}_n = \frac{\sum_i D_i N_i}{\sum_i N_i}$$

$$\overline{D}_w = \frac{\sum_i W_i D_i}{\sum_i W_i} = \frac{\sum_i D_i N_i D^3}{\sum_i N_i D^3} = \frac{\sum_i N_i D_i^4}{\sum_i N_i D_i^3}$$

$$P_D = \frac{\overline{D}_w}{\overline{D}_n}$$

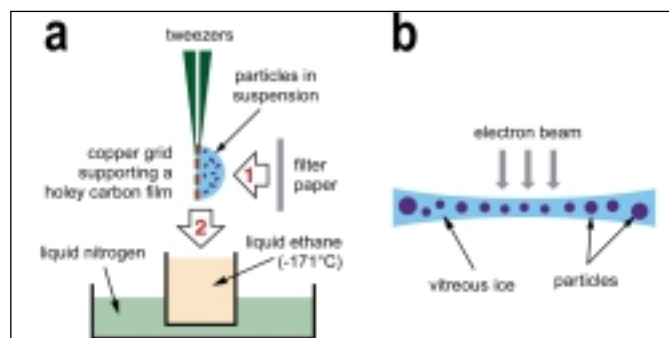where N_i is the number of particles at the ith class in the size-distribution histogram and W_i

Figure 1:
(a) Production of thin vitrified films for cryo-TEM: 1. The excess of suspension was blotted with a filter paper; 2. The grid was quench-frozen into liquefied ethane at -171°C. (b) Schematic transverse view of a vitreous ice film containing polymer particles.
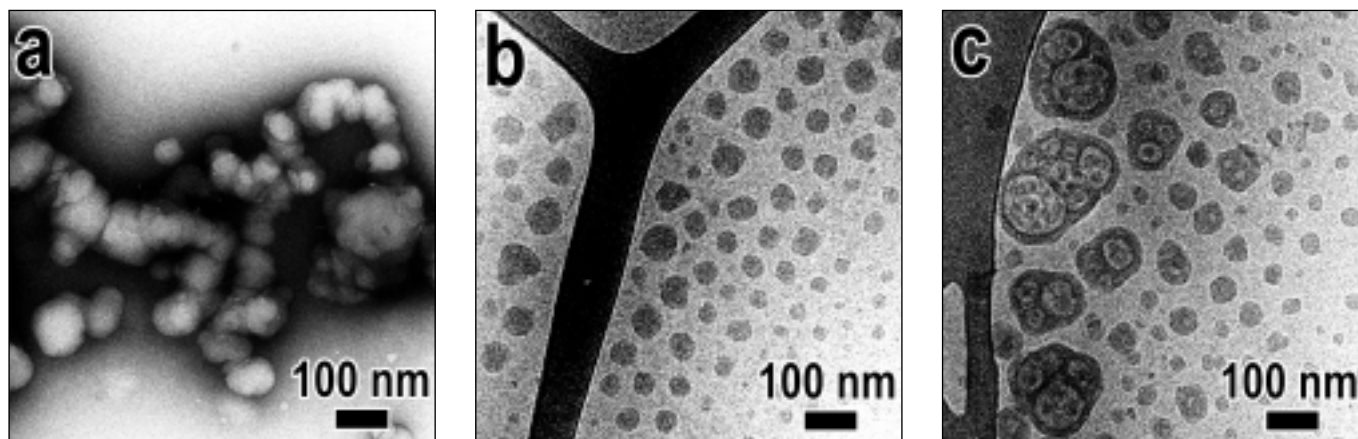
Figure 2:
(a) TEM image of polyurethane particles after negative staining. (b) Similar dispersion observed by cryo-TEM. (c) Cryo-TEM of a polymer dispersion with a different composition, showing particles with a complex inner morphology.

the molecular weight. For a more consistent comparison with the data obtained by DLS, a Z-average mean diameter was calculated from the TEM data as :

$$\overline{D}_{Z(TEM)} = \frac{\sum_i N_i D_i^6}{\sum_i N_i D_i^5}$$

For each sample, size-distribution histograms were determined from a total of about 1000 particles accumulated from several cryo-TEM images.

RESULTS AND DISCUSSION

TEM observation

Figure 2a shows polyurethane nanoparticles after negative staining with uranyl acetate. Since the glass transition temperature (Tg) of the polymer was lower than room temperature (varying from -60 to 0°C depending on the polymer composition), the soft particles could deform and flow during drying. Moreover, we could not decide whether the observed coalescence arose from a drying artifact or if such an aggregation existed in solution. The cryo-TEM image in Fig 2b clearly shows unaggregated spheroidal nanoparticles embedded in vitreous ice. More complex particles were also observed, as shown in Fig 2c, where the larger objects exhibit a peculiar nano-encapsulated morphology, suggesting that the pre-polymer synthesis and the chain extension could not form homogeneous nanospheres. This is a typical example where the direct visualisation of the dispersion provided information about the mechanism of particle formation, whereas DLS would be insensitive to this type of morphological feature.

Image analysis

The contrast between the polymer particles and the embedding ice was generally low in cryo-TEM images, partly due to the strong inelastic electron scattering. Contrast enhancements were performed but they also increased the contribution of the background noise from the negatives. On the other hand, variations in the ice thickness induced background intensity modulations. Consequently, the grey-level histogram of the cryo-TEM micrographs generally exhibited a broad peak (Fig 3a) and it was difficult to define luminance classes corresponding to specific contributions from the supporting membrane, the particles and the embedding medium. To limit these problems, the treatments were performed on smaller regions of interest (ROI) selected by the user (Fig 3b). To get a better contrast, the TEM micrographs were recorded with a negative defocus, generating fresnel fringes around the ice-embedded objects. Considering the high background noise, only a white fringe located outside of the particle surface could be seen. However, as we mostly used 1 to 2 mm defoci, we assumed that fresnel effects would not significantly influence the particle detection.

The main steps of the image processing procedure were:

1. Manual selection of a rectangular ROI (Fig 3b, step 1).
2. Local adaptive background smoothing to homogenise the luminance and improve object detection: this routine fits a polynomial surface to the sampled background and corrects the ROI luminance by subtracting this surface [8].
3. Manual thresholding based on a visual control, followed by an image binarisation (Fig 3b, step 2).
4. Elimination of background heterogeneities using successive erosions/dilatations.
5. Edge detection of the particles (Fig 3b, step 3) and separation process.

6. Fitting of the individual objects with equivalent ellipses, the diameter being calculated as the mean between major and minor axes.

In order to validate our semi-automatic procedure, we checked that 'manual' measurements performed on the same images and numbers of particles yielded similar results. However, as expected, the semi-automatic image analysis generally ran four times faster. An example or size distribution histogram is presented in Fig 4b.

Surface tension effects may influence the particle distribution during sample preparation. Controlling the thickness of the vitreous ice film is generally difficult and depends on the diluent composition (salts, surfactants, organic solvents), the room humidity level, the blotting efficiency, etc. Thickness values that are proper for TEM imaging typically vary from 50 to 200 nm [7]. The presence of a single layer of particles in the film is important, as illustrated in Fig 5a: the larger nanospheres are more or less isolated, while the smaller ones overlap along the observation axis. In that case, size-distribution analysis is hardly possible, although the operator still has a good general 'impression' on the suspension dispersity.

In addition, due to surface tension effects, the frozen film often exhibits a gradient of thickness. Consequently, the average background intensity in the image varies over the field of view. As explained earlier, binarisation can only be properly carried out after background fitting and correction. Another consequence is the fast reorganisation of the particles in the liquid film, just before freezing. The largest particles tend to accumulate near the edges of the carbon membrane where the water film is thicker. The smaller particles remain closer to the centre of the film. Depending on the local concentration and steepness of the gradient, regular distributions may be observed, the nanospheres reorganising along iso-thickness lines according to their size (Fig 5b). However, we cannot rule out the fact that some bigger objects may have migrated towards areas that are too thick for proper observation. These 'hidden' particles would thus be absent from the statistic treatment, which would yield an error in the mean diameter calculation. When the film

Table 1:
Mean diameters and polydispersity indexes calculated from cryo-TEM images and DLS experiments for four different polyurethane dispersions.

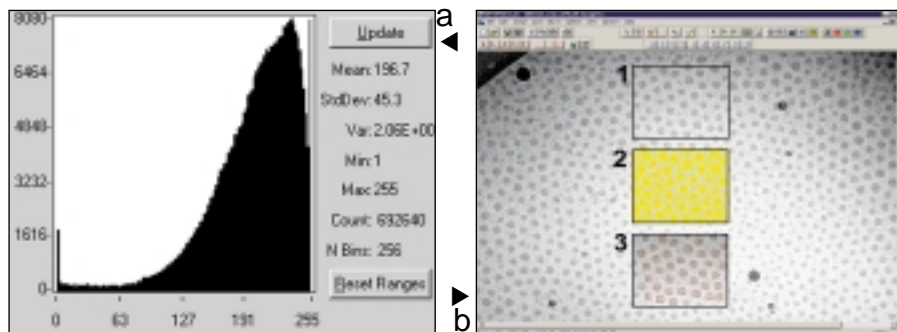| P_D	$\overline{D}_N$ nm	$\overline{D}_W$ nm	$\overline{D}_{Z(TEM)}$ nm	$\overline{D}_{Z(DLS)}$ nm
1.25	37.9	47.4	51.5	55.6
1.32	22.2	29.3	35.6	68.7
1.4	24.8	34.8	40.6	76.3
1.5	33.2	49.9	76.8	130.4

Figure 3:

(a) Grey-level histogram of a typical cryo-TEM image of ice-embedded polymer nanoparticles. (b) Stages of the semi-automatic procedure for particle size measurement: 1. manual selection of the ROI; 2. manual thresholding; 3. detection of the particles and fit by ellipses.

thickness is more or less constant, particles can mix more randomly, at the risk of overlapping (Fig 5a).

With a Tg lower than room temperature, the suspended nanoparticles are soft in the liquid film and thus sensitive to the surface tension effects. If their size in the dispersion is larger than the local thickness of the liquid film, and provided that they cannot 'migrate' to thicker areas, the nanoparticles are squeezed within the thin film. Their apparent diameter thus increases, yielding an incorrect spread of the size-distribution histogram towards larger diameters. Indeed, it is difficult to visualise such an effect and judge if the particles are actually deformed. In our experiments, we assumed that the particle size might be unreliable above 100-120 nm.

After binarisation, the image analysis algorithm performs several erosions/dilatations which, depending on the particle shape, may generate an error on the contours. This error was estimated to be around 1 pixel, i.e. 2 nm, considering our sampling rate. Moreover, the successive erosions, carried out during the image 'cleaning', eliminated objects smaller than 5-6 pixels. Consequently, particles smaller than 10 nm were not properly taken into account in our size-distribution histograms. This is readily visible in Fig 4b although the effect was not detected in most samples.

Finally, several remarks can be made when comparing the mean diameters obtained by DLS and image analysis. Values corresponding to four different dispersions with increasing polydispersity index P_D are given in Table 1. First of all, there is a significant difference between the values of $\overline{D}_N$ and $\overline{D}_{Z(DLS)}$ which increases at higher polydispersity. This could be expected, since the detection is based on different properties of the particles. In particular, DLS gives more statistical 'weight' to the larger particles which are more highly scattering objects. Moreover, DLS is sensitive to the ionic environment of the nanospheres that cryo-TEM cannot visualise since it has the same density as the embedding medium. The comparison of $\overline{D}_{Z(TEM)}$ (calculated from the cryo-TEM data as a D(6,5) statistical mean) with $\overline{D}_{Z(DLS)}$ is more relevant. $\overline{D}_{Z(DLS)}$ always appears to be larger than $\overline{D}_{Z(TEM)}$. The values are close when P_D is low, but the deviation becomes larger with increasing polydispersity. The fourth case, with P_D =1.50, perfectly illustrates how cautious one has to be to interpret and compare the data obtained with techniques sensitive to different properties of the particles.

CONCLUSION

In this work, several techniques were used concurrently to study aqueous dispersions of polyurethane nanoparticles. Light scattering was non-destructive and allowed us to characterise rapidly a large number of samples over a wide range of sizes. However, it showed some limitations in the case of polydisperse distributions and with particles smaller than 50 nm. The combined use of cryo-TEM and image analysis appeared to be complementary to DLS. In particular, the absence of aggregation as well as differences in nanoparticle morphology were important results provided by this direct visualisation. However, the size analysis of soft polymer particles only made sense for diameters below 100 nm. Moreover, the smaller objects (<10 nm) may not have been properly detected. These limits would obviously vary for different polymers, depending on factors such as particle density, crystallinity and Tg. In addition, the use of zero-loss energy-filtered imaging would certainly increase the contrast of cryo-TEM micrographs and consequently improve particle detection.

REFERENCES

1. Sudol E.D. and El Aasser M.S. In: Emulsion Polymerization and Emulsion Polymers, Lovell P.A., El-Aasser M.S. Eds, Wiley-Interscience, New-York, pp 699-722, 1997.
2. Putaux J.L. et al. Ultrastructural aspects of phytoglycogen from cryo-TEM and quasi-elastic light scattering. Int. J. Biol. Macromol. 26, 145-150, 1999.
3. Chalaye S. et al. Synthesis of composite latex particles filled with silica. Control of the composite particles composition. Macromol. Symp. 169, 89-96, 2001.
4. Collins E.A. Measurement of Particle Size and Particle Size Distribution. In: Emulsion Polymerization and Emulsion Polymers, Lovell P.A., El-Aasser M.S., Eds, Wiley-Interscience, New-York, pp 385-436, 1997.
5. Lahtinen M. et al. The chain extension of anionic prepolymers in the preparation of aqueous poly(urethane-urea) dispersions, Polym. Int. 52, 1027-1034, 2003.
6. Dubochet J. et al. Cryo-electron microscopy of vitrified specimens. Quart. Rev. Biophys. 128, 219-228, 1988.
7. Harris J.R. Negative Staining and Cryoelectron Microscopy: the Thin Films Techniques, Bios Scientific Publishers, Oxford, UK, 1997.
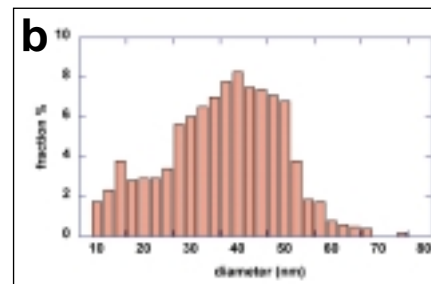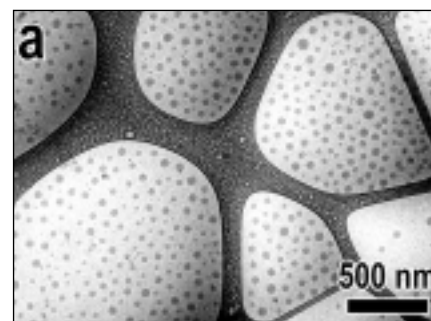8. Optimas user guide, Media Cybernetics, www.mediacy.com

Figure 4:

(a) Cryo-TEM micrograph of a polyurethane suspension. (b) Corresponding size-distribution histogram obtained by semi-automatic image analysis, for a total of about 1000 particles. The shoulder in the low diameter region suggests a bimodal distribution.
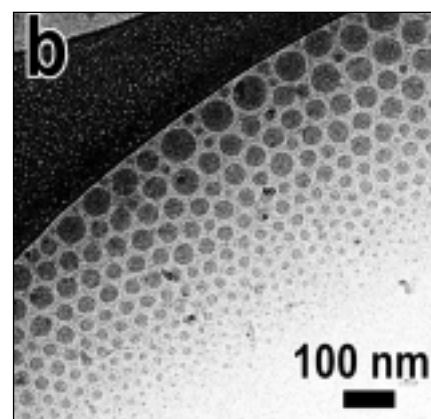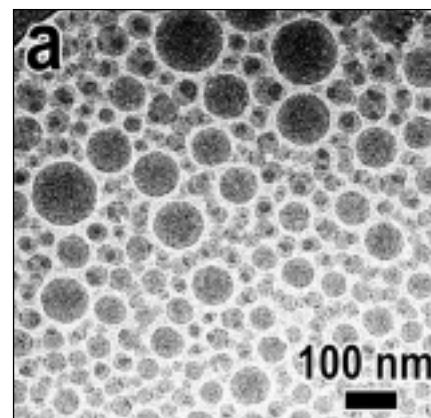

Figure 5:

Effect of the embedding liquid thickness on the distribution of polydisperse particles. (a) The thickness is more or less constant. Particles are mixed but the smaller ones overlap along the observation direction. (b) Regular reorganisation of the nanospheres in a thickness gradient. The larger particles are closer to the carbon membrane where the liquid film is thicker.